Understanding Function and Performance of Carbon Additives in Lead-Acid Batteries

D. G. Enos,[a] S. R. Ferreira,[b,*,z] H. M. Barkholtz,[c] W. Baca,[b] and S. Fenstermacher[d]

[a]*Materials Reliability, Sandia National Laboratories, Albuquerque, New Mexico 87123, USA*
[b]*Advanced Power Sources R&D, Sandia National Laboratories, Albuquerque, New Mexico 87123, USA*
[c]*Energy Storage Technology and Systems, Sandia National Laboratories, Albuquerque, New Mexico 87123, USA*
[d]*East Penn Manufacturing, Lyons, Pennsylvania 19536, USA*

While the low cost and strong safety record of lead-acid batteries make them an appealing option compared to lithium-ion technologies for stationary storage, they can be rapidly degraded by the extended periods of high rate, partial state-of-charge operation required in such applications. Degradation occurs primarily through a process called hard sulfation, where large $PbSO_4$ crystals are formed on the negative battery plates, hindering charge acceptance and reducing battery capacity. Various researchers have found that the addition of some forms of excess carbon to the negative active mass in lead-acid batteries can mitigate hard sulfation, but the mechanism through which this is accomplished is unclear. In this work, the effect of carbon composition and morphology was explored by characterizing four discrete types of carbon additives, then evaluating their effect when added to the negative electrodes within a traditional valve-regulated lead-acid battery design. The cycle life for the carbon modified cells was significantly larger than an unmodified control, with cells containing a mixture of graphitic carbon and carbon black yielding the greatest improvement. The carbons also impacted other electrochemical aspects of the battery (e.g., float current, capacity, etc.) as well as physical characteristics of the negative active mass, such as the specific surface area.
 [DOI: 10.1149/2.1031713jes]

Manuscript submitted August 24, 2017; revised manuscript received October 2, 2017. Published October 31, 2017.

Valve-regulated lead-acid (VRLA) batteries are a mature rechargeable energy storage technology. Low initial cost, well-established manufacturing base, proven safety record, and exceptional recycling efficiency make VRLA batteries a popular choice for emerging energy storage needs.[1,2] VRLA batteries are employed in stationary storage applications such as: utility ancillary regulation services, wind farm energy smoothing, and solar photovoltaic energy smoothing.[3] Stationary applications may require short duration, high-rate, and partial state-of-charge cycling (HRPSoC).[4] Under HRPSoC duty, conventional VRLA cells fail prematurely from irreversible $PbSO_4$ formation within the negative plates.[5] Regular cycling to 100% state-of-charge (SoC) mitigates $PbSO_4$ crystal formation and growth. However, regularly cycling to 100% SoC is not viable for many stationary storage applications. Large $PbSO_4$ crystals are not easily reduced back to metallic lead during HRPSoC charging, reducing cycle life. Reduced cycle life of VRLA batteries increases the operating cost, thereby limiting their practicality for stationary applications.

VRLA battery HRPSoC cycle life can be increased with carbon modification of the negative active material (NAM).[6–10] Adding carbon to the negative plate inhibits $PbSO_4$ crystal formation and/or limits $PbSO_4$ crystal growth.[11–13] The underlying mechanism responsible for reducing $PbSO_4$ formation/accumulation is dependent on the size of the $PbSO_4$ crystallites. Controlling $PbSO_4$ microstructure has been found to be difficult while maintaining low cost. Other methods exist to limit $PbSO_4$ crystal size; including utilization of a carbon honeycomb structure instead of traditional cast or punched grids.[14] For example, Kelly et al. have developed carbon foam-based grid technology that has demonstrated improved cycle life over conventional VRLA batteries.[15] This technology has limited commercial success due to increased manufacturing cost of carbon foam plates compared to conventional technology.

Recent work evaluated the impact of various carbon additives in the NAM of a VRLA battery, including novel nano-carbon materials.[6,7,9–11,13,16–25] Researchers have hypothesized that carbon contributes in one or more different aspects of battery performance. Chemical reactivity and surface area are important if the material is electrochemically active.[8,21] Carbon may also improve electrical conductivity within the NAM.[19] In this case, a conductive carbon network is important, benefitting from smaller particle diameters.[13] Certain carbon materials can act as a pseudo-capacitor absorbing excess charge and therefore enhancing electrochemical activity at the Pb/H_2SO_4 interface.[6,26] Additives may also work as an electro-osmotic pump transporting H_2SO_4 deep within the electrode, increasing utilization of the NAM.[6] Increasing the specific surface area of the NAM may boost performance by allowing more H_2SO_4 in the NAM.[16,21,27,28] Finally, carbon may reduce pore diameter within the NAM.[11]

While carbon additions have a favorable impact on HRPSoC cycle life, they can negatively impact other aspects of battery performance. Carbon displaces active material within the NAM, reducing initial cell capacity. Also, under normal operating conditions, carbon has a low hydrogen evolution over-potential.[24] This could increase the magnitude of parasitic side reactions such as water reduction, potentially increasing the rate of self-discharge and reducing the efficiency of charging. Finally, large specific gravity differences and poor grid adhesion may result in a non-uniform carbon dispersion within the NAM.[6,16,17,21,23,28]

In this work, VRLA battery cells were constructed with negative plates containing a series of different carbon additives, along with an unmodified control within a commercially available VRLA battery case, using standard fabrication processes. The carbon materials were selected such that a range of carbon morphologies and production methods were captured. Carbon additives were structurally and chemically characterized. Once the negative plates were formed, their physical properties were evaluated. Batteries were assembled using the control and carbon modified negative electrodes, along with a standard positive electrode. The electrochemical performance of the control and carbon-modified cells was then characterized using a series of standard protocols to determine their cycle life as well as overall behavior.

Experimental

Preparation of VRLA cells.—Negative VRLA cell plates were prepared using a standard commercial process and the associated equipment. Three carbon-modified NAMs were prepared, along with a standard control (i.e., no excess carbon). The carbons were selected to capture a range of different chemical and physical properties, including varying surface area and electrical properties, an underlying goal being to establish if one form or morphology was more beneficial than another. The carbons explored included an electrically conductive acetylene black, an activated carbon, and a combination

*Electrochemical Society Member.
[z]E-mail: srferre@sandia.gov

of carbon black and graphitic carbon. Once combined, pasted, and cured, the raw electrodes contain a mixture of PbO, $PbSO_4$, Pb°, expanders, and carbon. The carbon content of the NAM in the control battery was approximately 0.17 wt% (based upon the mass of PbO), the activated carbon loaded NAM material contained 1.5 wt%, the acetylene black carbon loaded NAM contained 1.0 wt% and the mixed graphitic/carbon black loaded NAM contained 2 wt% graphite, and 2 wt% carbon black.

All negative plates were electrochemically formed externally using standard commercial processes, prior to assembly of the battery. The control and carbon modified plates were assembled into batteries using an existing sealed six cell VRLA battery case design produced by East Penn Manufacturing. Each cell consisted of three negative plates and two positive plates. Between each positive and negative plate was a standard absorbed glass mat (AGM) 250g/m^2 separator (1.56 mm thick at a pressure of 10 kPa, tested per BCIS-03A (BCI Recommended Test Methods for VRLA-AGM Separators)).[29] The negative plates were 4.56 in (11.56 cm) high, 4.5 in (11.43 cm) wide, and 0.066 in (0.17 cm) thick, with a total of 67 g of unformed NAM per plate. The positive plates were the same width and height, but were 0.110 in (0.28 cm) thick, with a total of 108.0 g of unformed positive active material (PAM) per plate. A stack pressure of 57.7 kPa (23.2% compression) was used for the batteries. The plate geometry and count within each cell resulted in an estimated initial capacity of 10 Ah. While the entire six cell commercial battery case was populated with plates, only a single cell was filled with electrolyte. The fill electrolyte was H_2SO_4 with a starting specific gravity of 1.295 g/cm^3, increased to 1.302 g/cm^3 through the addition of Na_2SO_4. Once the cell was filled, the battery case was sealed, and the cell connected to external leads. As such, the electrochemical results reported here represent the behavior of a single cell containing three negative plates and two positive plates.

Physical characterization.—Scanning electron microscopy (SEM) was used to evaluate the physical structure of the carbon additives and battery plates. X-ray diffraction (XRD) was used to evaluate crystal structure of the carbon additives. Brunauer, Emmett, and Teller (BET) surface area measurements were performed on the carbon additives and battery plates. The acid-soluble impurity content within carbon additives was assessed using inductively coupled plasma-mass spectroscopy (ICP-MS). Water soluble anions were detected via ion chromatography. Acid soluble contaminants were extracted in 6N HCl. Anions were extracted by sonicating a known quantity of each carbon in high purity water and analyzing the leachate.

Physical structure of the carbon-modified and control plates was assessed in both the raw and formed conditions. In all cases the center negative plate was characterized to avoid complications from plate position. Cross-sections were taken from each sample at the top, center, and bottom, mounted using traditional metallographic techniques, and imaged in the SEM. Lead sulfate distribution within the structure was evaluated by cathodoluminescence (CL). A Zeiss variable pressure secondary electron (VPSE) detector captures SEM features that light up via CL. When impacted by an electron beam, $PbSO_4$ will luminesce. Metallic lead does not luminesce, allowing for easy detection of $PbSO_4$. As the intensity of the luminescence was not characterized, CL was used to qualitatively identify when $PbSO_4$ was present, rather than to quantify the amount of $PbSO_4$ present. Mercury porosimetry was used to evaluate the overall degree of porosity and the pore size distribution within each plate in the as-received, formed, and cycled conditions. Cycled values were obtained after 1 k cycles, 10 k cycles, and upon cell death. Samples for both mercury porosimetry and BET surface area were taken from the center of the plate, adjacent to where the center cross section described above was taken. The locations where each sample was taken are shown schematically in Figure 1. It should be stressed than only a single example of each cell was evaluated at each cycle count, and as such the data should be considered qualitatively as the uncertainty associated with each measurement could not be quantified.

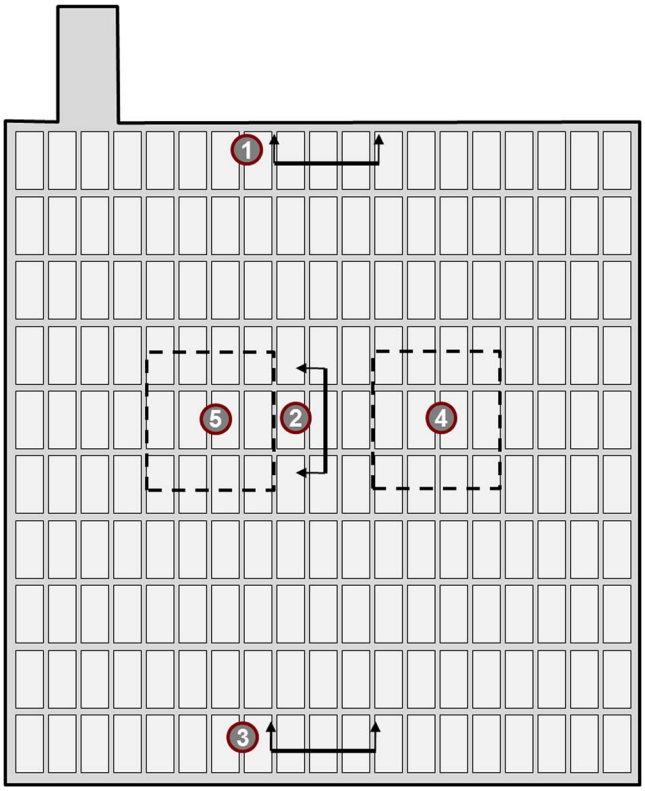

Figure 1. Center plate cross section locations. Locations 1, 2, and 3 were used for SEM imaging of the active material structure. Location 4 was removed for Hg porosimetry and location 5 for BET surface area measurements. The negative plates were 4.555 in. (11.56 cm) high, 4.5 in. (11.43 cm) wide, and 0.066 in. (0.17 cm) thick, with a total of 67g of unformed NAM per plate.

Electrochemical measurements.—*Baseline electrochemical performance measurements.*—Baseline electrochemical performance of each cell was evaluated. The cell was charged at 2.3 V (with a maximum current of 1C) until the current fell to 75 mA. After a one-hour rest at open circuit, the cell was discharged at 1C to 1.75 V. The total electrical charge passed during discharging was recorded. After another hour-long rest at open circuit, the cell was recharged to 108% of the discharge capacity. After another rest, each cell was discharged at 1C to 1.75 V. This second discharge capacity was logged as the initial capacity, and used as a baseline. The open circuit voltage (OCV) and impedance of each cell was measured.

Float current measurements.—The float current is a measure of the rate of reactions which occur during the overcharge of the battery. These reactions include oxygen evolution and potentially grid corrosion at the positive plate, along with oxygen recombination and hydrogen evolution at the negative plate.[6] Float currents of each cell type were measured at five voltages. Cells were first charged at 2.45 V for 24 hours, then allowed to stabilize for 48 hours. Each cell was then held at 2.27 V for ten days and the final current measured. This process was repeated at potentials of 2.30 V, 2.35 V, 2.40 V, and 2.45 V for periods of 72 hours, 24 hours, 12 hours, and 6 hours respectively.

Hybrid pulsed power characterization measurement.—The hybrid pulsed power characterization (HPPC) test, as defined in the FreedomCAR Battery Test Manual[30] was performed on pristine (i.e., untested) examples of each cell type. The HPPC test aims to establish the ability of a battery to deliver power or accept charge as a function of SoC over the useable voltage range.

Six month self-discharge measurement.—The rate at which the control and carbon-modified cells self-discharge was evaluated. An

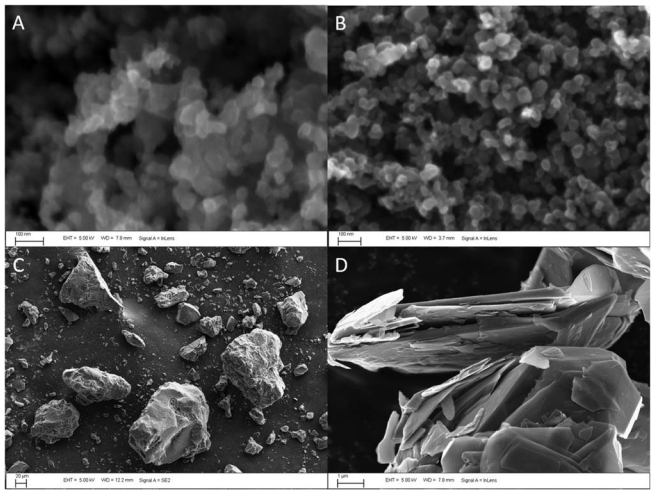

Figure 2. SEM images of (A) acetylene black, (B) carbon black, (C) activated carbon, and (D) graphitic carbon. Legends differ and are shown in the lower left hand corner of each image (100 nm, 100 nm, 20μm, 1μm respectively).

example of each cell type was charged to full capacity using the procedure described above. After charging, each cell sat without any externally applied load for a period of six months under ambient laboratory conditions. At the end of this six-month rest period, the capacity was measured again and compared to the initial capacity.

Cycle testing measurements.—Examples of each cell type were cycled under HRPSoC duty, simulating ancillary regulation services for a wind farm energy smoothing application.[31] HRPSoC cycle tests use 10% discharge cycles centered around a 50% SoC. Cycling is performed at a rate of 1C to 2C, providing maximum power and energy performance. At 1 k and 10 k cycles, batteries were destructively disassembled and plate structure was evaluated. Batteries were disassembled within a glove box containing an inert (i.e., nitrogen) atmosphere. Immediately after being removed from the battery case, the plates were rinsed with deionized water and allowed to dry within the glove box. Once dried, samples were taken from each plate for analysis, as illustrated in Figure 1. A portion of the battery cells evaluated in this study contained a Hg/Hg_2SO_4 reference electrode in the VRLA electrolyte. Half-cell potentials were found and utilized to pinpoint effects of HRPSoC duty on positive versus negative active materials.

Remaining cells were cycled to irreversible failure. Cells were cycled per the procedure defined above until failure, with failure defined as a reduction in capacity to below 80% of initial capacity, and then a recovery charge was employed. Each recovery charge involved charging to 108% initial capacity and served to decrease $PbSO_4$ presence. After multiple recovery charges, the cells could not be recovered, and were considered irreversibly failed. BET surface area and Hg porosimetry was performed at the first failure and after multiple recovery charges.

Results and Discussion

Structural and chemical analysis of carbons.—There are many types of carbon, each with unique physical features. Even within a carbon type wide variations exist, such as: particle diameter, aggregation size/shape, BET surface area, porosity, contaminants, etc.[17] These properties influence VRLA performance and NAM structure. To draw conclusions about effects of carbon-modification, precursor materials were characterized. Physically, acetylene black (Figure 2A) and carbon black (Figure 2B) are similar. Both consist of approximately 20–30 nm diameter aggregates. The activated carbon (Figure 2C) consisted of micrometer-sized particles with a glassy appearance. Glassy appearance is consistent with high-temperature activated carbon.[32] Graphitic carbon (Figure 2D) contains numerous graphite platelets with a typical particle size on the order of tens of microns.

X-ray diffraction patterns for each of the carbon additives were used to characterize the crystallinity and structure of each carbon additive. Graphitic carbon is well-ordered hexagonal graphite (type 2H). The pattern for activated carbon was consistent with an amorphous structure; supporting the visual observation of a glassy appearance. The patterns for acetylene black and carbon black were similar to that of graphite, with significant peak broadening and larger d-spacing. Shift in spacing and considerable peak broadening suggest a fine crystal size. The XRD spectra from both materials are a mixture of nano-crystalline and amorphous peaks. This was most easily observed in carbon black which had two different peak profiles. Acetylene black peak profile fitting resolved two discrete peaks, but peak broadening made peak location and broadening difficult to determine.

Based upon their similar particle size, the acetylene black and carbon black were expected to have the same specific surface area. BET specific surface areas of acetylene black and carbon black were found to be 75.0 ± 0.2 and 73.7 ± 0.1 m^2 g^{-1}, respectively. The graphitic carbon exhibited a lower specific surface area than either the carbon black or acetylene black, at 6.84 ± 0.2 m^2 g^{-1}. Activated carbon yielded a specific surface area of 2060 ± 4 m^2 g^{-1}, significantly larger than the other three. The reason for this large difference is the microscopic structure of the activated carbon. Being derived from wood, it is highly porous, and thus the actual surface area is vastly larger than the macroscopic particle size.

Acid and water soluble contaminant species are of particular interest due to the H_2SO_4 electrolyte within VRLA cells. Detrimental species, such as iron, may act to poison electrochemical reactions. Both acetylene black and graphitic carbon had minimal acid or water soluble contaminant present. The carbon black contained a significant quantity of sulfate and sodium present, but no species were noted that would adversely impact battery performance. Activated carbon had a variety of contaminants present, including 100 ppm Fe (potentially detrimental), as well as significant concentrations of sodium and phosphate. As the activated carbon was derived from wood, soluble contaminants were anticipated.

Electrochemical performance.—Open circuit voltage (OCV) and internal impedance (Table I) were nominally identical between the cells. Average discharge capacity of each of the cell type was measured for 15 batteries. Control cells, which are based on optimized production processes, have the tightest distribution of capacities, as illustrated in Figure 3 and Table I. Carbon-modified batteries have greater distribution and lower initial capacity. Carbon displaces some of the active material, thus reducing overall active material within the cell. Carbon-modified batteries increase capacity upon cycling except for activated carbon, discussed later. The increase in capacity observed upon cycling indicates that the carbon additives inhibited charge acceptance during formation.

Float current measures the electrochemical activity during overcharge of the cell. As discussed above, the reactions that contribute to the float current may include oxygen evolution and grid corrosion at the positive electrode, along with oxygen recombination and hydrogen evolution at the negative plate.[6] In all cases, float current increases upon carbon-modification of the NAM, as shown in Table I. The increase is likely the result of the parasitic side reactions discussed above. Oxygen recombination serves to chemically discharge the negative plate while it is being electrochemically charged.[33] This depresses the negative plate potential and causes an incomplete charge.[34] Increasing average float current with carbon modification agrees with depressed initial cell capacity documented in Table I.

Hybrid Pulse Power Characterization (HPPC) testing establishes the ability of the battery to deliver power or accept charge as a function of the SoC. The test was performed on new/uncycled cells. All four cell types behave similarly under HPPC conditions, as illustrated in Figure 4.

Carbon modified cells typically have a higher electrochemically active surface area. While this is beneficial under HRPSoC conditions

Table I. Key electrochemical performance data for each cell type studied here.

	OCV (V)	Impedance (μΩ)	Average Initial Capacity (Ah)	Average 10,000 Cycle Capacity (Ah)	Float Current at 2.45 V (mA)	Average Cycles to Failure
Control	2.147 ± 0.002	1997 ± 30	11.8 ± 0.2	11.1 ± 0.1	127 ± 6	17372 ± 5793
Acetylene Black	2.141 ± 0.008	2015 ± 36	11.6 ± 0.3	12.1 ± 0.2	199 ± 17	46172 ± 13430
Activated Carbon	2.158 ± 0.003	2038 ± 36	11.0 ± 0.4	10.3 ± 0.3	159 ± 2	29255 ± 5737
Graphitic Carbon and Carbon Black	2.146 ± 0.005	2114 ± 20	10.6 ± 0.4	12.20 ± 0.04	166 ± 10	50796 ± 13741

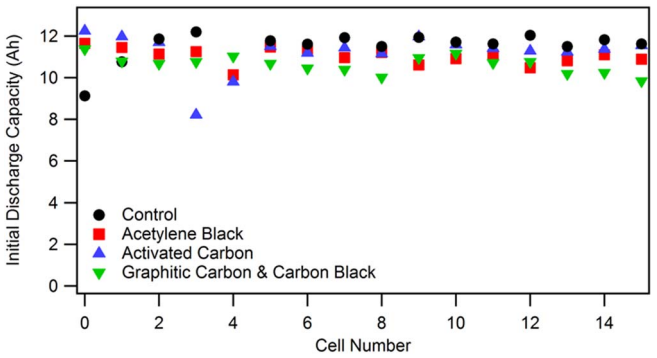

Figure 3. Initial 1C discharge capacity for the control and each of the carbon containing cell types.

to extend life; a disadvantage is that the carbon can serve as cathodic surface area within the NAM, increasing self-discharge. The control cell lost 22 ± 2% of its initial capacity due to the six-month self-discharge, the smallest loss of all batteries tested. Acetylene black, activated carbon, and graphitic carbon and carbon black containing cells lost 30 ± 5%, 25 ± 6%, and 39 ± 6%, respectively. The electrochemically active carbon within the carbon modified cells serves as a local cathode within the NAM, driving lead dissolution and contributing to the increased self-discharge rates.

HRPSoC cycling rapidly degrades VRLA batteries. Simulating these conditions, HRPSoC testing was carried out on all cell types. Figure 5 shows the negative half-cell potential on charging. The control, Figure 5A, loses charge acceptance over time. This effect is more pronounced when acetylene black, Figure 5B, or activated carbon, Figure 5C, were included in the NAM. No decay was noted when the combination of graphitic carbon and carbon black were added to the NAM, Figure 5D. It has been proposed that graphitic flakes capture electrons which reduce $PbSO_4$ to metallic lead.,[18,25] and as such, the graphitic carbon additive may be responsible for the observed increase in HRPSoC performance.

Reduction in charge acceptance after cycling is likely from $PbSO_4$ crystal formation. After 10 k cycles, compositions began to distinguish themselves electrochemically. Capacity loss was evident in the control and activated carbon batteries (see Table I). Conversely, acetylene black had slightly higher capacity at 10 k cycles than initial. Graphitic carbon and carbon black substantially increased capacity at 10 k cycles. Increased capacity at 10 k cycles demonstrates resilience under HRPSoC duty. Average cycle life for each cell type is summarized in Table I.

Structural analysis of negative plates.—The impact of carbon-modification on the structure of the NAM was studied by taking metallographically prepared cross sections and evaluating them in the SEM. Figure 6 contains images from each plate type. Cylindrical/fibrous materials observed in all plates are the binder. Acetylene black particles were not visible within the structure due to their nanoscale diameter (Figure 6B), though there were dark, carbon rich heterogeneities observed, indicative of particle aggregation. Activated carbon particles are large and readily visible within the structure, Figure 6C. More detailed evaluation of the large activated carbon particles revealed metallic lead within fissures and pores present in the activated carbon, suggesting this carbon species is electrochemically active. Graphitic carbon is visible in Figure 6D whereas the carbon black is not. As with acetylene black, heterogeneity is indicative of carbon black aggregation.

As shown in Figures 7A and 7B, both overall pore volume and pore size, assessed via mercury porosimetry, increase as the plate is formed. Distribution of pore size shifts to larger values for all plates except when containing graphitic carbon and carbon black. Graphitic carbon may add rigidity to the NAM, preserving initial pore structure. While the overall distribution shifted to larger pores, for all of the carbon modified plates, a portion of the distribution was maintained in the small 1–2 μm range. Pore size distribution was also monitored as a function of cycle life, illustrated in Figures 7C and 7D. Again, the carbon-modified plates maintained a distribution of small pores throughout the period monitored here, as will be discussed in more detail below. Pore structure resilience is strongly correlated to cycle life.[22] Small diameter pores hinder the formation of large $PbSO_4$ crystallites, resulting in a distribution of small $PbSO_4$ crystals that are more easily dissolved/reduced during charging. Additionally, pore diameters below 1.5 μm can act as a semi-permeable membrane, restricting mass transport of SO_4^{2-} and HSO_4^- into the pore. As a result, the Pb^{2+} formed during discharge of the battery in these

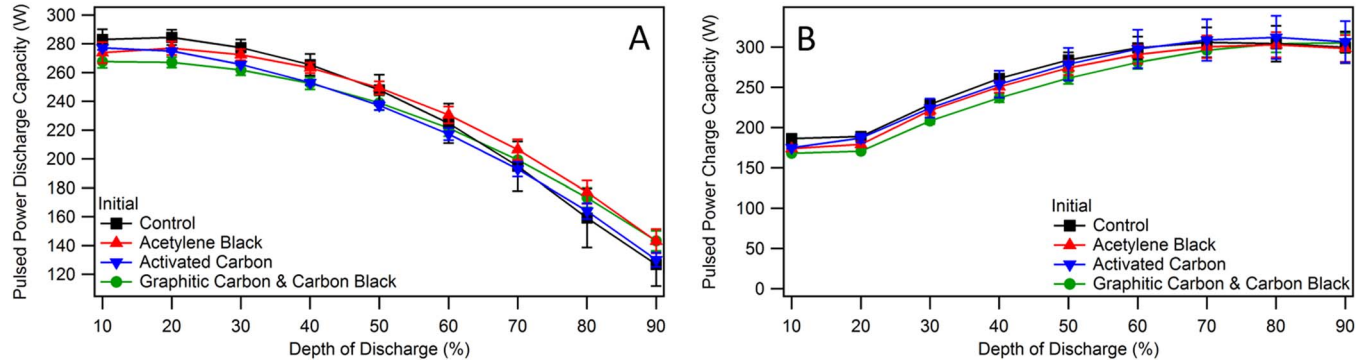

Figure 4. Results of HPPC (A) discharge and (B) charge on fresh cells.

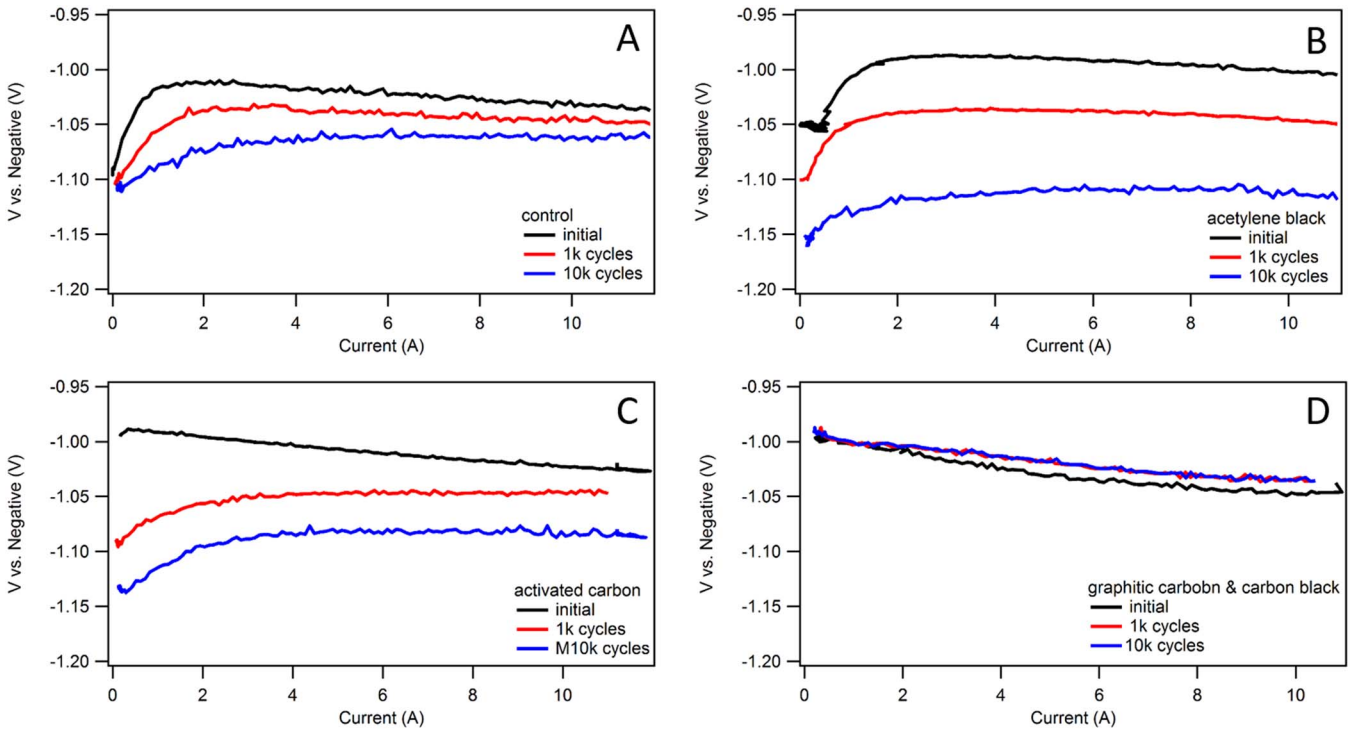

Figure 5. Negative electrode half-cell during charging for (A) control, (B) acetylene black, (C) activated carbon, and (D) graphitic carbon and carbon black containing cells.

small pores hydrolyzes, forming $Pb(OH)_2$, which then transforms into α-PbO precipitate on the pore walls.[7]

Under HRPSoC duty cycling, reactions between active material and electrolyte take place within pores.[35] Decreased pore volume and surface area is evidence of incomplete charge acceptance, reducing cell capacity. BET surface area of each cell type was evaluated initially, after 1 k cycles, 10 k cycles, failure, and recovery. No significant changes in overall surface area were noted for the control, acetylene black, or graphitic carbon and carbon black NAM. Activated carbon containing cells exhibited decreasing surface area with cycling. Additionally, activated carbon did not benefit from recovery charging. Decreasing surface area is likely from progressive hard surface sulfation.

Figure 7C and Figure 7D illustrate pore size distribution after 1 k and 10 k cycles, respectively. After 1 k cycles, all carbon containing batteries had pore sizes centered around 1 to 2 μm. The control has a portion around 3 μm and a large fraction closer to 7.5 μm. At 10 k cycles, the control cell lost small pores and was composed primarily of 7–10 μm pores. Activated carbon behaved similarly, with most pores around 7–10 μm. As $PbSO_4$ crystals form and grow, pore diameters expand to accommodate them.[20] This process of plate oxidation is called expansion, and is a well-known failure mechanism. Contrarily, both acetylene black and graphitic carbon and carbon black batteries remained unchanged at 1 k and 10 k cycles, with pores around 1–2 μm, indicative of increased stability afforded to the NAM by these carbon formulations.

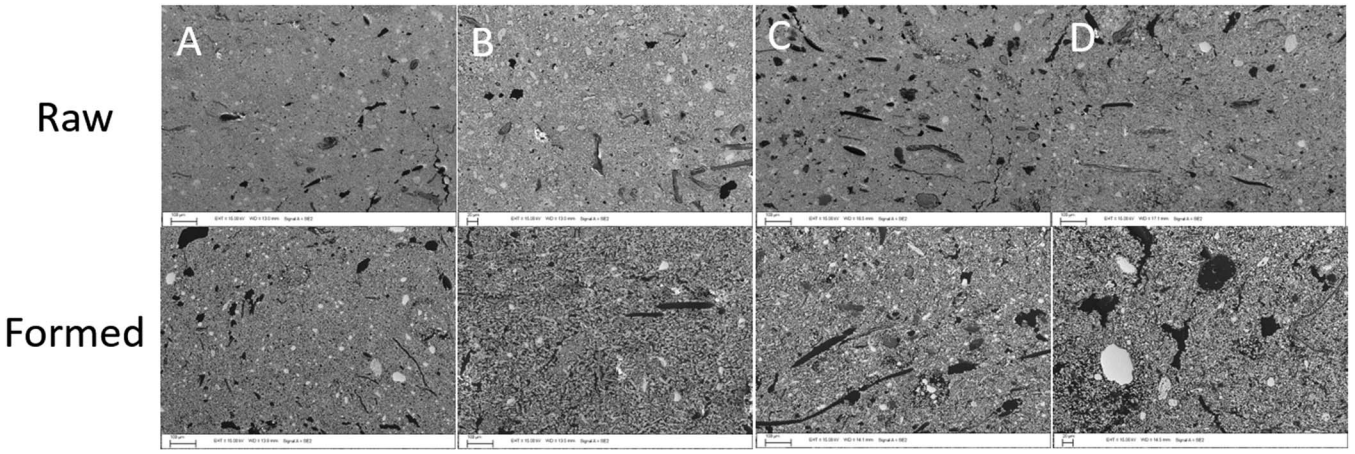

Figure 6. Cross sectional SEM images of negative plates containing (A) nothing – control plate, (B) acetylene black, (C) activated carbon, and (D) graphitic carbon and carbon black. Each plate was imaged in two forms; raw (top) and formed (bottom). Scale bars for B (top) and D (bottom) are 20 μm, all others are 100 μm.

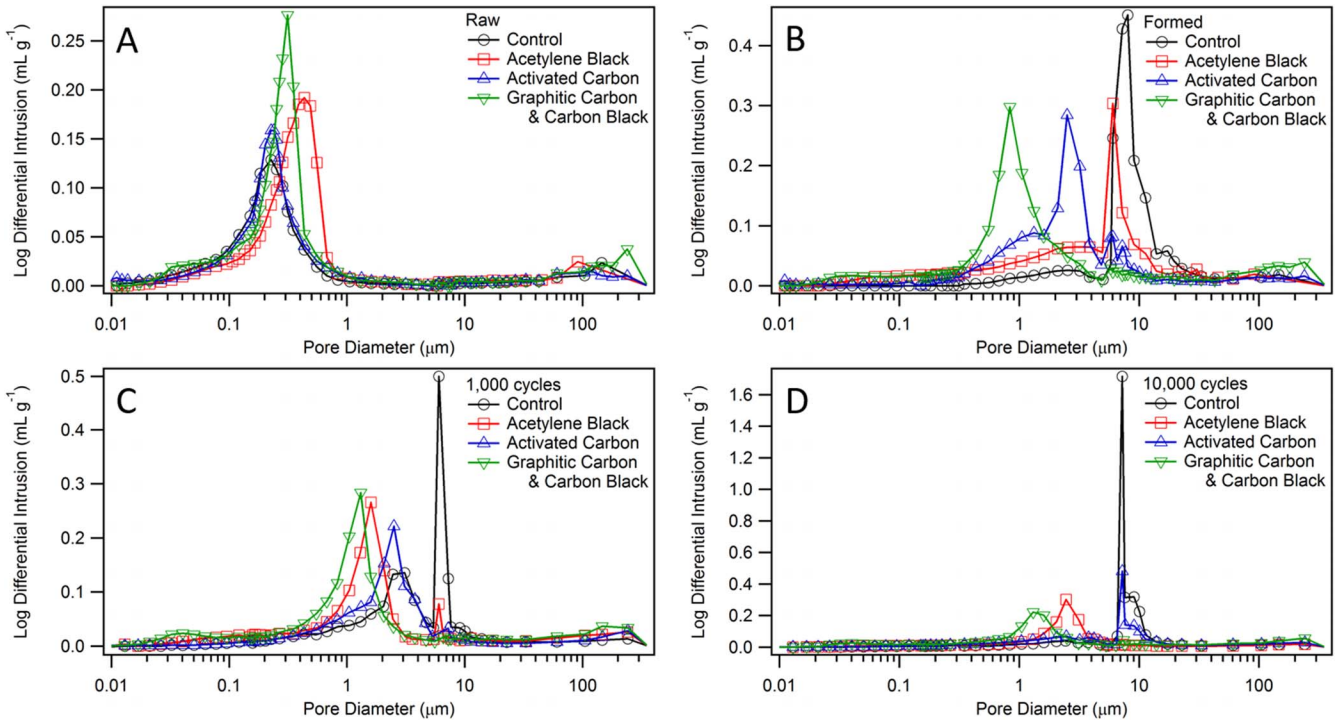

Figure 7. Pore size distribution of (A) raw, (B) formed, (C) 1,000 times cycled, and (D) 10,000 times cycled negative plates with different carbon additives alongside the unmodified control.

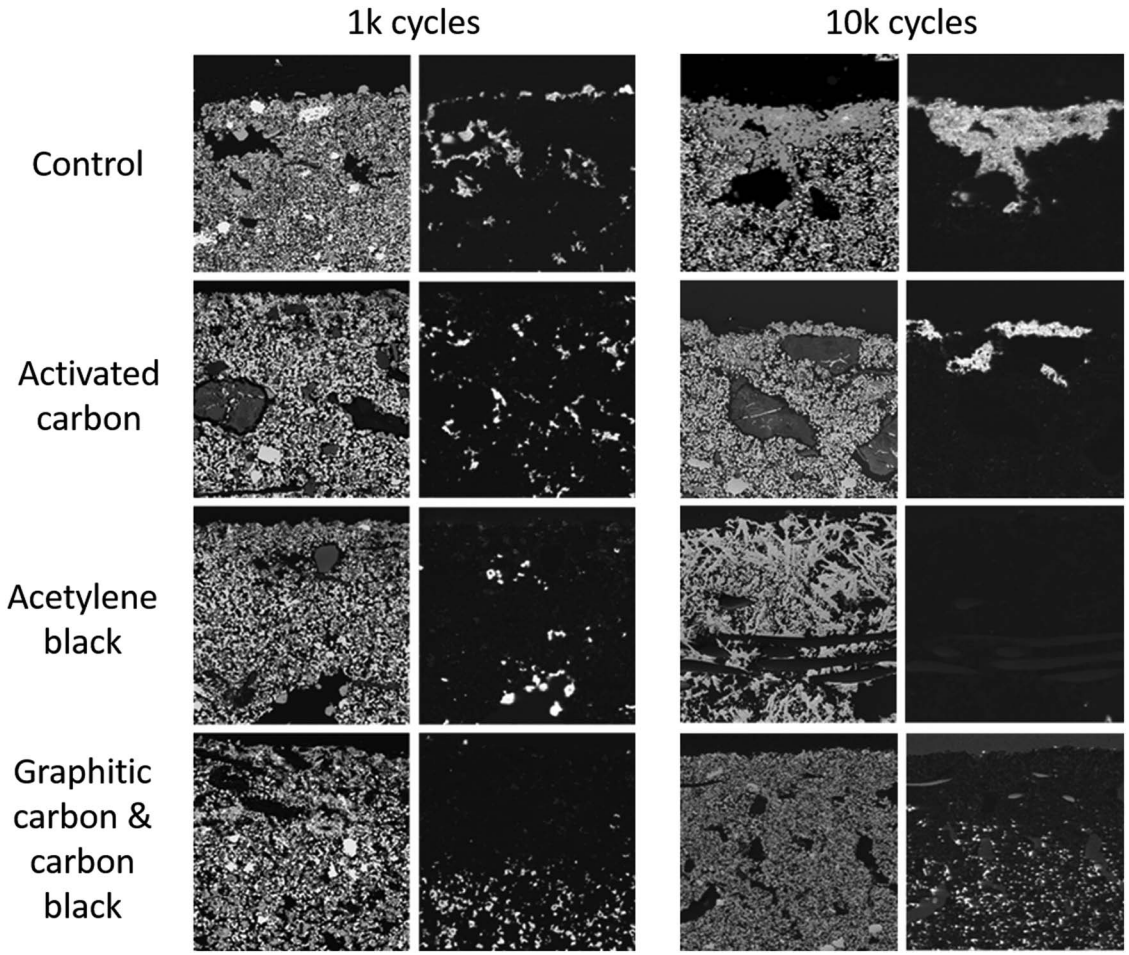

Figure 8. Cross sectional SEM images from each cell type after 1 k and 10 k cycles. The left column is a backscattered SEM image and the right is a CL image of the same location. Field of view for all images is approximately 264 microns for all but the graphitic carbon and carbon black at 10 k cycles, where it is 633 microns.

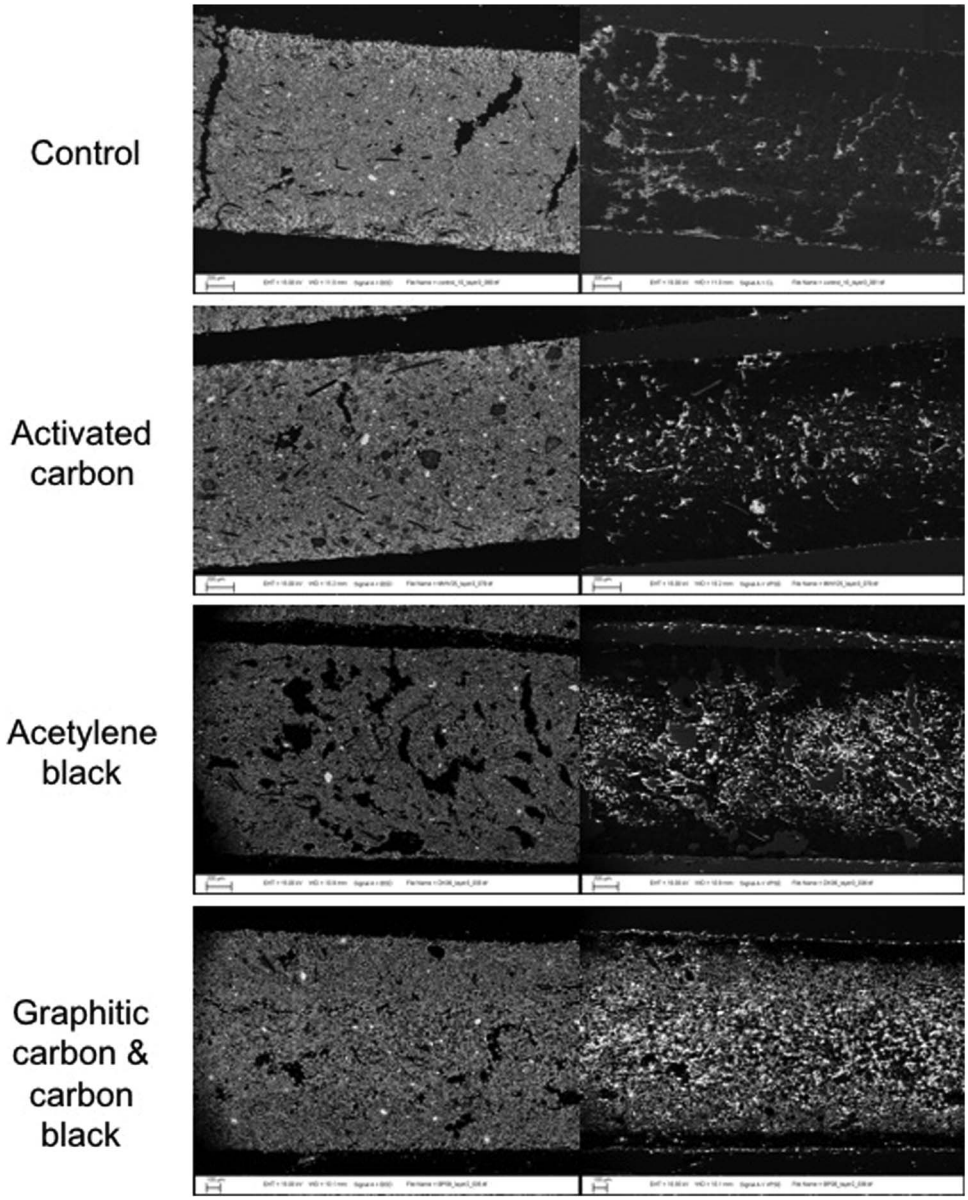

Figure 9. SEM images after failure. The left image is a backscattered electron SEM image, while the right image is a cathodoluminescence (CL) image of the same area. Scale bars are 100 μm for graphitic carbon and carbon black NAM and 200 μm for all other images.

SEM images of plate materials at 1 k cycles is shown in Figure 8 (left). The control cell possessed a globular structure similar to initial images. CL showed $PbSO_4$ crystals distributed through the plate, with a thin layer on the plate surface. This is the beginning of hard sulfation. Carbon containing cells have notably less $PbSO_4$ present on the plate surface. In none of the carbon-modified cases was a $PbSO_4$ layer visible on the plate surface. Graphitic carbon and carbon black had $PbSO_4$ in the center of the plate and the surface was completely clear.

At 10 k cycles many differences between the cell types are seen, Figure 8 (right). The control cell was within several thousand cycles of average failure (Table I) and had significant surface hard sulfation. Hard sulfation is accelerated under HRPSoC cycling. Activated carbon also had signs of hard sulfation, though not as severe as the control. In addition, $PbSO_4$ appeared to form primarily near surface activated carbon particles. Comparing to observations made via Hg porosimetry, it is speculated that the $PbSO_4$ is plugging smaller pores associated with activated carbon. At 10 k cycles acetylene black was markedly different than other batteries in terms of its physical structure, which appeared dendritic. The plate was also clear of lead sulfate. Presumably, acetylene black helped reduce $PbSO_4$ to Pb which accumulated non-uniformly within the cell. Non-uniformity likely caused local polarization differences and therefore the reduced half-cell charging illustrated in Figure 5B. Although heterogeneous, no $PbSO_4$ is present at 10 k cycles, increasing cell capacity from initial as indicated in Table I. Graphitic carbon and carbon black appeared nominally identical to 1 k cycles. $PbSO_4$ is visible at the center of the plate and the surface was completely clear. This behavior is consistent with another report of graphitic carbon modified cells under HRPSoC duty.[17] Perhaps resilience to $PbSO_4$ formation is from synergistic effects of graphitic carbon and carbon black. Carbon black is structurally similar to acetylene black and should behave similarly in the NAM. Acetylene black alone caused heterogeneous deposition of Pb, forming dendrites. Graphitic carbon may increase NAM rigidity, resisting dendrite formation. Combining graphitic carbon and carbon black yields a 'best of both worlds' scenario and best performance under HRPSoC duty.

Cells were then cycled to failure. The number of cycles to failure shown in Table I varied considerably across cell types. Graphitic carbon and carbon black containing cells had the longest cycle life.

This is expected as minimal electrochemical and structural changes were observed at 1 k and 10 k cycles. Acetylene black also had a long cycle life. Although Pb dendrites were observed, $PbSO_4$ was not. Next longest cycle life was the activated carbon containing cells, follow by the control. Average cell cycle life of the graphitic carbon and carbon black containing cells was roughly twice that of the control. Previously published reports state unmodified VRLA cells survive about 25,000 HRPSoC cycles.[17] This is within range of the control reported here. Wide cycle life range was noted for both the control and carbon containing batteries and is unlikely from incomplete cell production process optimization. Incorporating recovery charges each time a cell failed increased the cycle life of all compositions except activated carbon, and potentially contributed to a wider distribution in cycle life. This relationship occurs because the earlier a cell failed the more effective the recovery is expected to be to mitigate large $PbSO_4$ crystals.

Analysis of the batteries at failure did not reveal conclusive evidence in terms of accelerated aging. Structurally, failure showed an increase in what was observed at 10 k cycles, as illustrated in Figure 9. In the graphitic carbon and carbon black and acetylene black containing plates a sizeable population of large voids developed, indicating plate expansion. The degree of sulfation at the plate surface, and size of sulfate particles formed throughout the plate, appear to have been minimized in acetylene black and graphitic carbon and carbon black. Recovery charges cleared out $PbSO_4$ crystals within pores, as larger pore diameters increased after recovery. Additionally, the positive plates were characterized as a function of cycles. The structure does not become occluded or otherwise altered with cycling. Positive plates are not responsible for cell failure as determined by SEM of failed plates and half-cell reactions.

Conclusions

VRLA batteries were prepared using standard commercial processes, materials, and the associated equipment. A control containing no excess carbon and three carbon-modified NAMs were prepared. The carbons were selected to capture a range of different chemical and physical properties, including varying surface area and electrical properties, an underlying goal being to establish if one form or morphology was more beneficial than another. The control cells and carbon-modified cells were evaluated under a range of conditions, from basic electrochemical performance through HRPSoC cycling. Physical and chemical changes within the batteries were monitored as a function of cycles and correlated to performance. Based upon the results of this study, the following can be concluded with respect to carbon additions:

- All carbon additions reduced initial cell capacity, with the most severe reduction observed for the combination of graphitic carbon and carbon black. Capacity increased in the carbon modified cells with cycling, exceeding that of the control battery. This effect was likely a combination of reduced active material (displaced by adding carbon) and that the carbon additions also inhibited initial charge acceptance.
- All carbon modified cells exhibited an increased float current, suggesting that the carbon increased the NAM surface area, and with it parasitic side reactions.
- All carbon modified cells exhibited an increased self-discharge rate. This increase was likely due to the electrochemically active area of the carbon, serving as local cathodic sites to drive self-discharge of the NAM.
- All carbon modified cells exhibited superior HRPSoC cycle performance when compared to the control. Graphitic carbon and carbon black had the most significant impact, and activated carbon had the smallest impact.
- Charge acceptance as a function of HRPSoC cycling was maximized by the addition of graphitic carbon and carbon black. The control, active carbon, and acetylene black carbon modified cells all exhibited reduced charge acceptance with cycling, with the activated carbon and acetylene black undergoing a more significant reduction than the control.
- BET surface area was constant for the control, carbon black plus graphite, and acetylene black containing cells across their entire cycle life. The surface area decreased with cycles for the activated carbon containing cells, but was always much greater than the other battery chemistries.
- The pore structure for the control, acetylene black, and activated carbon containing cells all evolved over their cycle life, approaching a common distribution. The carbon black plus graphite containing cell remained relatively constant over its entire cycle life.

Acknowledgments

This work was funded by the US DOE OE′s Energy Storage Program. The authors thank Dr. Imre Gyuk for his support of research advancing safety in stationary energy storage. Special thanks to Rod Shane of East Penn Manufacturing for cell materials used in this work, also to Bonnie McKenzie for significant technical support on SEM and cathodoluminescence imaging, Denise Bencoe for BET and Hg Porosimetry measurements, Alice Kilgo for metallographic analysis, Mark Rodriguez for X-ray diffraction, and Ted Borek for soluble contamination analysis. Additionally, the authors wish to recognize Tom Hund, Kyle Fenton, and Armando Fresquez for helpful technical discussions. Finally, recognitions to Marie Dosanjh for her technical writing expertise.

Sandia National Laboratories is a multi-mission laboratory managed and operated by National Technology and Engineering Solutions of Sandia, LLC., a wholly owned subsidiary of Honeywell International, Inc., for the U. S. Department of Energy's National Nuclear Security Administration under contract DE-NA-0003525. SAND No. SAND 2017-4182 J.

ORCID

S. R. Ferreira https://orcid.org/0000-0002-5852-1525
H. M. Barkholtz https://orcid.org/0000-0001-7997-7567

References

1. J. Yang, C. Hu, H. Wang, K. Yang, J. B. Liu, and H. Yan, *International Journal of Energy Research*, **41**, 336 (2016).
2. L. Lam, R. Louey, N. Haigh, O. Lim, D. Vella, C. Phyland, L. Vu, J. Furukawa, T. Takada, and D. Monma, *Journal of Power Sources*, **174**, 16 (2007).
3. B. B. McKeon, J. Furukawa, and S. Fenstermacher, *Proceedings of the IEEE*, **102**, 951 (2014).
4. D. Conover, S. Ferreira, A. Crawford, D. Schoenwald, and V. Viswanathan, *PNNL-22010 Rev*, **1** (2014).
5. L. Lam, N. Haigh, C. Phyland, and A. Urban, *Journal of Power Sources*, **133**, 126 (2004).
6. P. Moseley, *Journal of Power Sources*, **191**, 134 (2009).
7. D. Pavlov and P. Nikolov, *Journal of Power Sources*, **242**, 380 (2013).
8. D. Pavlov, P. Nikolov, and T. Rogachev, *Journal of Power Sources*, **195**, 4444 (2010).
9. D. Pavlov, P. Nikolov, and T. Rogachev, *Journal of Power Sources*, **196**, 5155 (2011).
10. D. Pavlov, T. Rogachev, P. Nikolov, and G. Petkova, *Journal of Power Sources*, **191**, 58 (2009).
11. M. Calabek, K. Micka, P. Křivák, and P. Bača, *Journal of Power Sources*, **158**, 864 (2006).
12. K. Nakamura, M. Shiomi, K. Takahashi, and M. Tsubota, *Journal of Power Sources*, **59**, 153 (1996).
13. M. Shiomi, T. Funato, K. Nakamura, K. Takahashi, and M. Tsubota, *Journal of Power Sources*, **64**, 147 (1997).
14. A. Kirchev, N. Kircheva, and M. Perrin, *Journal of Power Sources*, **196**, 8773 (2011).
15. K. C. Kelley and J. J. Votoupal, *Battery Including Carbon Foam Current Collectors*, in, US Pat. No. 6979513 (2005).
16. P. Bača, K. Micka, P. Křivík, K. Tonar, and P. Tošer, *Journal of Power Sources*, **196**, 3988 (2011).
17. D. Boden, D. Loosemore, M. Spence, and T. Wojcinski, *Journal of Power Sources*, **195**, 4470 (2010).
18. U. Hasse and F. Scholz, *Electrochemistry Communications*, **3**, 429 (2001).
19. A. Hollenkamp, W. Baldsing, S. Lau, O. Lim, R. Newnham, D. Rand, J. Rosalie, D. Vella, and L. Vu, *Overcoming Negative-Plate Capacity Loss in VRLA Batteries Cycled Under Partial-State-of-Charge Duty*, in *Proceedings of Advanced Lead-Acid Consortium*, Research Triangle Park, NC. USA (2000).

20. K. Micka, M. Calábek, P. Bača, P. Křivák, R. Lábus, and R. Bilko, *Journal of Power Sources*, **191**, 154 (2009).
21. P. Moseley, R. Nelson, and A. Hollenkamp, *Journal of Power Sources*, **157**, 3 (2006).
22. M. Saravanan, P. Sennu, M. Ganesan, and S. Ambalavanan, *Journal of The Electrochemical Society*, **160**, A70 (2013).
23. M. Spence, D. Boden, and T. Wojcinski, *Identification of the Optimum Specification for Carbon to be Included in the Negative Active MAterial of a Valve-Regulated Battery in Order to Avoid Accumulation of Lead Sulfate During High-State-Charge Operation*, in *Proceedings of Advanced Lead-Acid Battery Sonsortium*, Research Triangle Park, NC, USA (2010).
24. P. Tong, R. Zhao, R. Zhang, F. Yi, G. Shi, A. Li, and H. Chen, *Journal of Power Sources*, **286**, 91 (2015).
25. N. Zakharchuk, S. Meyer, B. Lange, and F. Scholz, *Croatica Chemica Acta*, **73**, 667 (2000).
26. A. Jaiswal and S. C. Chalasani, *Journal of Energy Storage*, **1**, 15 (2015).
27. A. Hollenkamp, W. Baldsing, S. Lau, O. Lim, R. Newnham, D. Rand, J. Rosalie, D. Vella, and L. Vu, *Overcoming Negative-Plate Capacity Loss in VRLA Batteries Cycled inder Partial-State-of-Charge Duty*, in *Proceedings of Advanced Lead-Acid Battery Consortium*, Research Triangle Park, NC. USA (2002).
28. L. Lam, H. Ceylan, N. Haigh, T. Lwin, C. Phyland, D. Rand, and D. Vella, *Influence of residual elements on the oxygen-and/or hydrogen-gassing rates of lead-acid batteries*, in *Proceedings of the Advanced Lead-Acid Battery Consortium*, Research Triangle Park, NC, USA (2002).
29. BCIS-03A, in *Battery Technical Manual*, Battery Council International (Rev. September 2009).
30. E. Karden, S. Ploumen, B. Fricke, T. Miller, and K. Snyder, *Journal of Power Sources*, **168**, 2 (2007).
31. T. Hund, N. Clark, and W. Baca, *DOE Energy Storage Systems Research Program Annual Peer Review*, 2 (2006).
32. J. Zhao, L. Yang, F. Li, R. Yu, and C. Jin, *Carbon*, **47**, 744 (2009).
33. K. R. Bullock, *Journal of Power Sources*, **195**, 4513 (2010).
34. S. Misra, T. Noveske, S. Mraz, and A. Williamson, *Journal of Power Sources*, **95**, 162 (2001).
35. A. Mariani, K. Thanapalan, P. Stevenson, and J. Williams, in *Automation and Computing (ICAC), 2013 19th International Conference on*, p. 1 (2013).